# Impact of WSR-88D Scanning Strategies on Severe Storm Algorithms

RODGER A. BROWN

*NOAA/National Severe Storms Laboratory, Norman, Oklahoma*

JANELLE M. JANISH

*NOAA/National Severe Storms Laboratory and Cooperative Institute for Mesoscale Meteorological Studies, University of Oklahoma, Norman, Oklahoma*

VINCENT T. WOOD

*NOAA/National Severe Storms Laboratory, Norman, Oklahoma*

(Manuscript received 8 April 1999, in final form 17 August 1999)

ABSTRACT

The operational meteorological community generally recognizes that the greater spatial and temporal resolution of WSR-88D volume coverage pattern (VCP) 11 is preferable to VCP 21 when using algorithms to identify severe storm characteristics. The coarser vertical sampling of storms with VCP 21 likely produces less accurate results. An experiment was conducted to investigate the comparative effects of VCPs 11 and 21. Since VCP 21 is nearly a subset of VCP 11, the appropriate elevation angles were deleted from two VCP 11 datasets to produce proxy datasets for VCP 21 (called VCP 22). Various WSR-88D operational algorithms and National Severe Storms Laboratory prototype severe storm algorithms were run on the VCP 11 and VCP 21/22 datasets. At heights above 5° elevation angle, where VCP 21/22 had missing elevation angles relative to VCP 11, the majority of algorithm parameters had different values at least 50%–70% of the time. Therefore, this study confirms that VCP 11—not VCP 21—should be used in those convective storm situations where there is a contribution to critical warning parameters from elevation angles greater than 5°.

## 1. Introduction

The Weather Surveillance Radar-1988 Doppler (WSR-88D) currently uses two different volume coverage patterns (VCPs) for monitoring convective weather. VCP 11 consists of 14 elevation scans (ranging from 0.5° to 19.5°) in 5 min. VCP 21 consists of nine elevation scans (also ranging from 0.5° to 19.5°) in 6 min. Many WSR-88D users prefer VCP 11 when storms are within about 150 km of the radar owing to its enhanced vertical and temporal resolution. However, others prefer to use VCP 21 owing to its slightly more accurate estimates of reflectivity and Doppler velocity. It is generally felt that the poorer vertical resolution of VCP 21 is the primary factor that degrades the output from WSR-88D algorithms. Witt (1997) studied variations in velocity-based algorithm output from two different WSR-88Ds that viewed the same storm. One radar used VCP 11, and the other used VCP 21. Where there were significant algorithm differences between the two radars, Witt attributed the differences to the coarser vertical resolution of VCP 21.

Using data from two WSR-88Ds, it is difficult, in general, to separate the effects of VCP vertical resolution from other effects (such as range differences) on algorithm performance. Accordingly, an experiment was conducted to make some objective comparisons of the effect of vertical resolution on the two VCPs. In section 2, the approach and procedures used are discussed. Section 3 compares output from four WSR-88D algorithms and two refined algorithms developed at the National Severe Storms Laboratory (NSSL). Section 4 contains summary comparisons of 17 parameters from the six algorithms.

## 2. Procedure

The approach used was to produce a proxy VCP that was a good approximation to VCP 21. As shown in Table 1, the lowest five elevation angles are the same for VCPs 11 and 21. For elevation angles greater than 5.0°, the VCP 21 elevation angles differ by 0.6°, at most, from the corresponding VCP 11 elevation angles. Since

*Corresponding author address:* Dr. Rodger A. Brown, National Severe Storms Laboratory, 1313 Halley Circle, Norman, OK 73069. E-mail: brown@nssl.noaa.gov

TABLE 1. Comparison of elevation angles (°) for VCP 11, VCP 22 (modified VCP 11), and VCP 21.

| VCP 11 | VCP 22 | VCP 21 |
|---|---|---|
| 0.5 | 0.5 | 0.5 |
| 1.45 | 1.45 | 1.45 |
| 2.4 | 2.4 | 2.4 |
| 3.35 | 3.35 | 3.35 |
| 4.3 | 4.3 | 4.3 |
| 5.25 | — | |
| 6.2 | 6.2 | 6.0 |
| 7.5 | — | |
| 8.7 | — | |
| 10.0 | 10.0 | 9.9 |
| 12.0 | — | |
| 14.0 | 14.0 | 14.6 |
| 16.7 | — | |
| 19.5 | 19.5 | 19.5 |

essentially VCP 21 is a subset of VCP 11, the proxy dataset was produced by deleting the data at those VCP 11 elevation angles that are not close to those in VCP 21. The elevation angles for the proxy VCP, called VCP 22, are listed in the middle column of Table 1.

WSR-88D datasets from two diverse regions of the country were used to evaluate algorithm performance for VCPs 11 and 22. The first dataset was collected by the Melbourne, Florida (KMLB), radar from 1947 to 0755 UTC on 25–26 March 1992. At the beginning of the dataset, isolated convection was occurring over the southern portion of Florida. A line of storms was also starting to move across the northern portion of the peninsula from the northwest. Large hail (2–7.5-cm diameter; 0.75–3.0 in.) and damaging winds (some associated with short-lived bow echoes) were associated with the line as it moved southeastward across the peninsula. By the end of the period, all of the convective activity had moved over the Atlantic Ocean.

The second dataset was collected by the Frederick, Oklahoma (KFDR), radar from 1044 to 2319 UTC on 8 May 1993. Within the KFDR coverage area, there were broad areas of longitudinal convective lines and isolated multicell and supercell storms. All lines and storms moved to the northeast. Large hail (2–7-cm diameter; 0.75–2.75 in.) and strong winds were associated with the storms throughout the period. Tornadoes (F0–F1) were associated primarily with the supercells and a pronounced squall line that formed late in the period.

For this study, no attempt was made to follow individual reflectivity cells, mesocyclones, or tornadic vor-

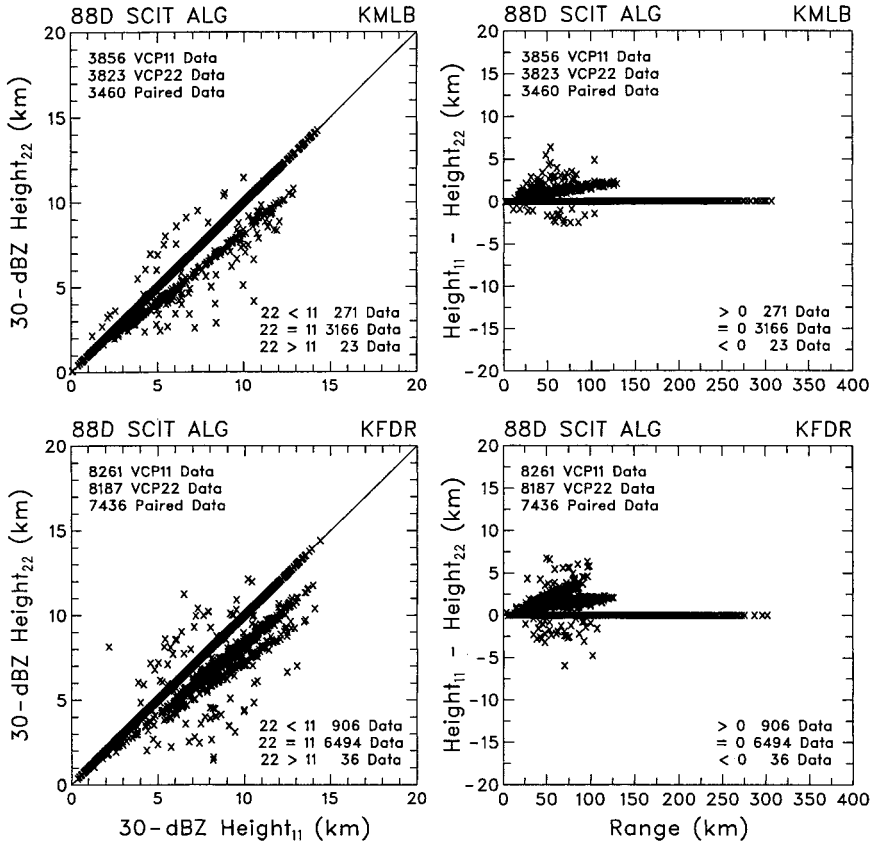


FIG. 1. Plots of 30-dB*Z* heights and height differences between VCP 11 and VCP 22 (designated by subscripts) for data collected by KMLB and KFDR. The cause of the radial bands is discussed in the text.

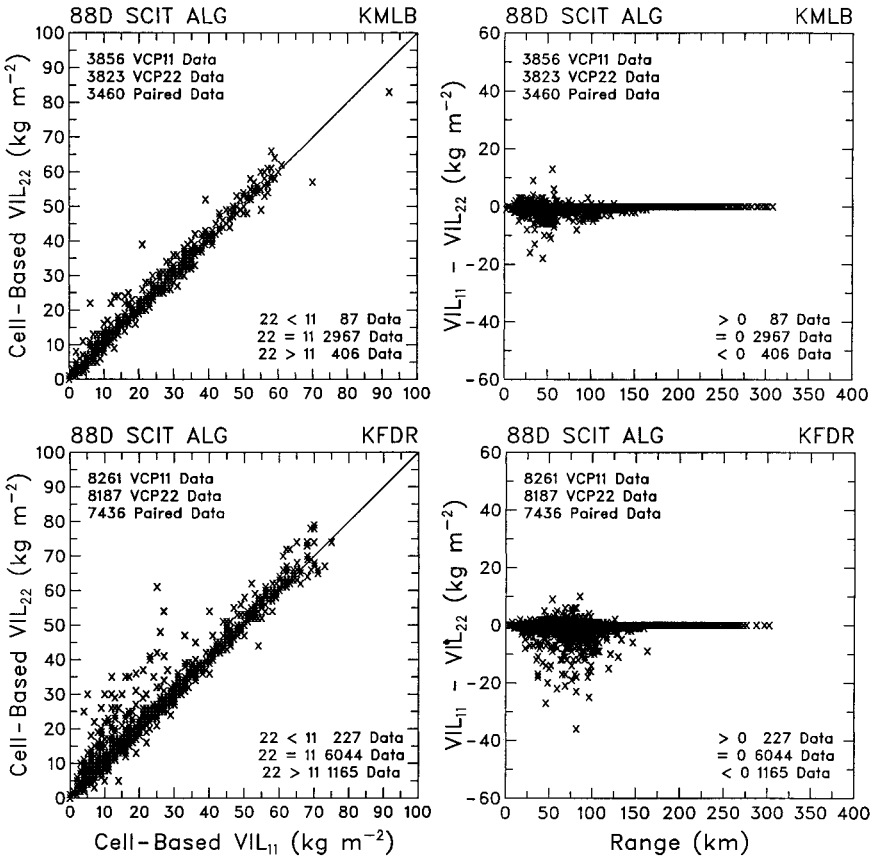


FIG. 2. Plots of VIL and VIL differences between VCP 11 and VCP 22 (designated by subscripts) for data collected by KMLB and KFDR.

tex signatures with time. Therefore, if an entity lasted for 12 volume scans, it was counted separately for each of the 12 volume scans. Consequently, when the total number of detected features is listed, the total is significantly larger than the number of identified cells, mesocyclones, or tornadic vortex signatures.

## 3. Comparison of VCPs 11 and 22

The utility of VCP 21 was evaluated by comparing proxy VCP 22 algorithm output with that of VCP 11. The values of algorithm parameters used for the comparisons came from data files that were written to disk when the algorithms were run on the archive level II radar datasets using the NSSL's Radar Algorithm and Display System. The following WSR-88D algorithms were selected for comparison: the storm cell identification and tracking (SCIT) algorithm, the hail detection algorithm (HDA), the mesocyclone algorithm (MESO), and the velocity azimuth display (VAD) algorithm. Two new algorithms developed by NSSL also were used: the mesocyclone detection algorithm (MDA) and the tornado detection algorithm (TDA). Other algorithms were not selected for comparison because the data files written to disk did not contain adequate information to identify the same feature in both VCPs. The results of the VCP 11–VCP 22 comparisons for these algorithms are discussed below.

### *a. Storm cell identification and tracking algorithm*

The SCIT algorithm (e.g., Johnson et al. 1998) identifies the existence and characteristics of individual storm cells. The algorithm also tracks and forecasts the three-dimensional centroid positions of the cells. An objective way to compare cell identification and tracking for VCPs 11 and 22 could not be devised using the available algorithm output. However, inspection of the displayed tracks showed that the vast majority of identified cells and their tracks were identical. Other SCIT parameters were used for VCP 11 and 22 comparisons. They are maximum reflectivity, height of the maximum reflectivity, maximum height of 30 dB*Z*, and vertically integrated liquid (VIL). Only plots of the comparisons of the 30-dB*Z* height and of VIL are presented in this paper.

Shown in Fig. 1 are the 30-dB*Z* height comparisons. The top of the figure shows data from KMLB, and the bottom of the figure shows data from KFDR. The left panels show scatterplots of values for the two VCPs.

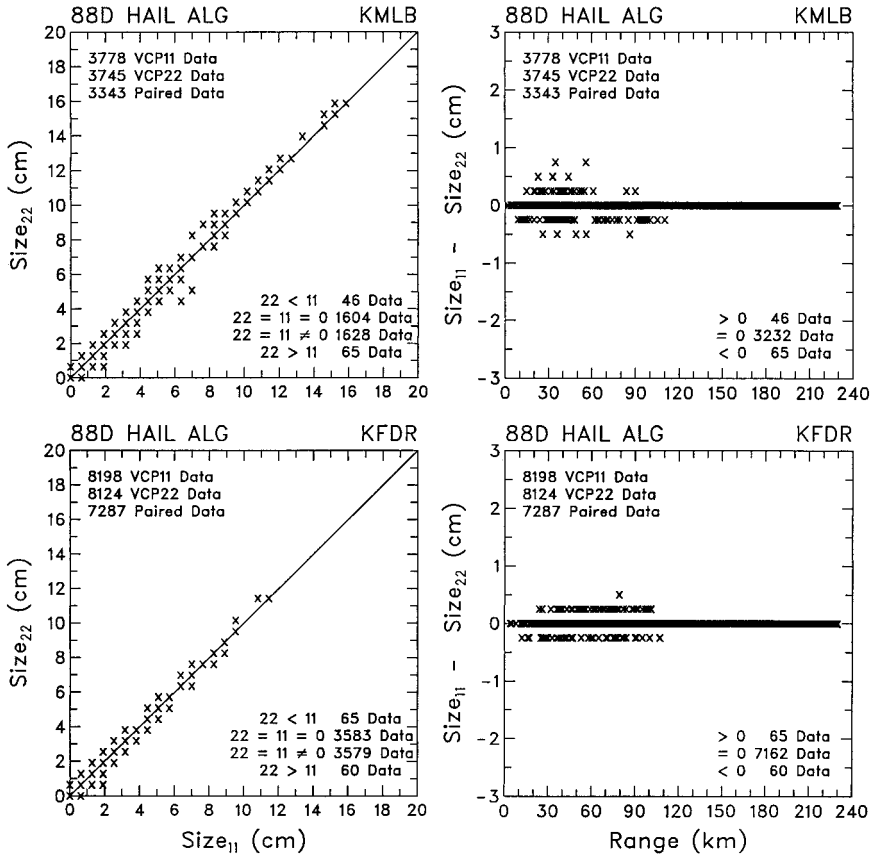


FIG. 3. Plots of maximum expected hail size and size differences between VCP 11 and VCP 22 for data collected by KMLB and KFDR.

The right panels show the differences between VCP 11 and VCP 22 values as a function of range. Listed in the upper-left corner of each panel are the number of VCP 11 data points, the number of VCP 22 data points, and the number of VCP 11 and 22 data point pairs that occurred at the same range and azimuth for a given volume scan; only paired values are used in the figures. Listed in the bottom-right corner of the left panels are the number of paired data points where the VCP 11 value is greater than, equal to, or less than the VCP 22 value. Listed in the bottom-right corner of each right panel are the same numbers as in the left panels, but they are expressed in terms of differences between the VCP 11 and 22 values.

For nearly all of the height pairs in Fig. 1 where the heights are not equal, the VCP 22 tops are lower than the VCP 11 tops. The missing elevation angles with VCP 22 can account for this situation. It is not clear why some VCP 22 tops are higher than the VCP 11 tops (less than 1% of the cases). Note that the differences between the parameter values at ranges greater than about 130 km are zero. This occurs because all of the pertinent data are at common elevation angles below 5.0° as indicated in Table 1.

Note in Fig. 1 that some plotted values are concentrated into bands radiating outward from the origin. These bands are a consequence of some of the missing VCP 22 elevation angles, relative to VCP 11. There are three distinct groupings of elevation angle differences that can arise between VCP 11 elevation angles and the closest VCP 22 elevation angle: 0.95/1.3°, 2.0°, and 2.5/2.7/2.8°. The dense band in the KMLB data is due to elevation angle differences of 0.95/1.3°. The two dense bands in the KFDR data are due to differences of 0.95/1.3° and 2.5/2.7/2.8°. These radial bands of concentrated data points occur only with height parameters. Since there are many combinations of height differences that can specify depth, none of the depth plots have unique radial bands.

As a measure of the liquid water in a vertical column in the storm, VIL depends on the vertical profile of reflectivity (Greene and Clark 1972). Instead of VIL being computed in vertical columns, as originally proposed, this algorithm computes it from the maximum reflectivity at each level within an identified storm cell. This ''cell-based'' approach allows for tilting reflectivity cores (e.g., Johnson et al. 1998).

Shown in Fig. 2 are plots of cell-based VIL. For those VIL values that are not equal for VCP 11 and 22, most of the ones associated with VCP 22 are greater (by 10–

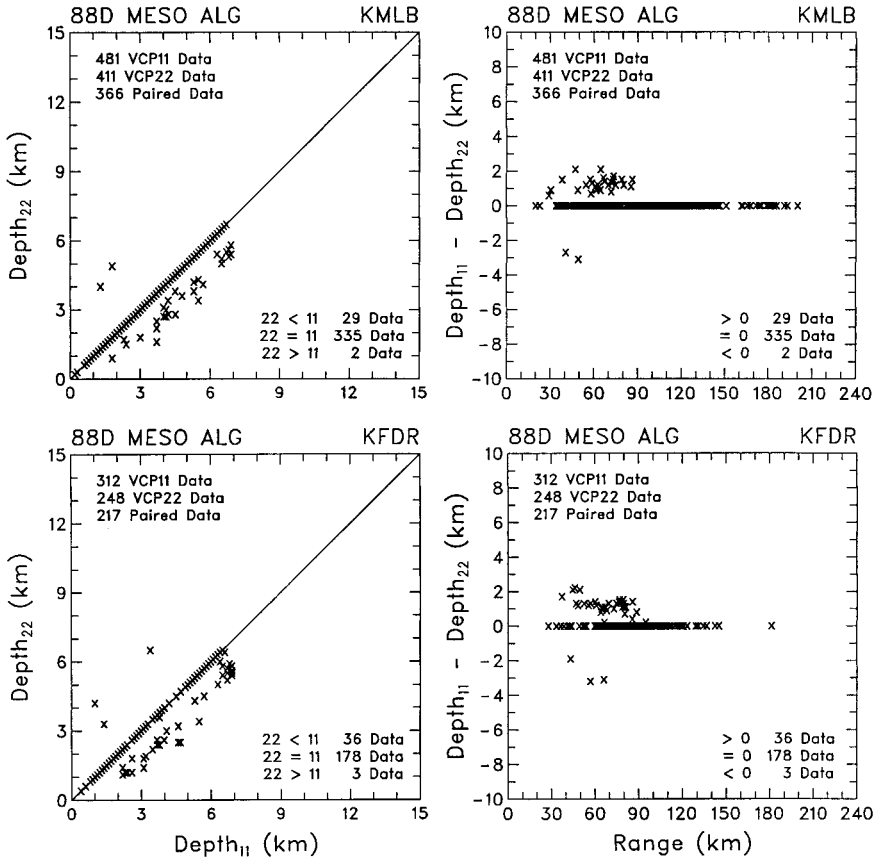


FIG. 4. Plots of mesocyclone depth and depth differences between VCP 11 and VCP 22 for data collected by KMLB and KFDR. The plots are based on the WSR-88D mesocyclone algorithm.

20 kg $m^{-2}$) than those associated with VCP 11. Initially, this may seem to be a bit strange, since VCP 22 has a few deleted elevation angles. However, as part of the vertical integration process, the maximum reflectivity at each elevation angle is assigned to a depth extending from halfway to the adjacent lower elevation angle to halfway to the adjacent higher elevation angle. If the maximum reflectivity in the storm occurs at a VCP 22 elevation angle above 5°, that value is assigned to a greater depth than for the same VCP 11 elevation angle (see Mahoney and Schaar 1993).

For plots of maximum reflectivity values (not shown) within each storm, with one or two exceptions, the VCP 22 values are less than or equal to VCP 11 values. One expects to find this relationship because some VCP 11 maximum reflectivity values occur at elevation angles that are missing in VCP 22. Plots of the height of maximum reflectivity values (not shown) reveal that of the few pairs that do not have the same values, most of the VCP 22 values underestimated those associated with VCP 11.

### *b. WSR-88D hail detection algorithm*

Witt et al. (1998) discuss the characteristics of the WSR-88D HDA. Three parameters produced by HDA were investigated: maximum expected hail size, probability of hail, and probability of severe hail. Only plots of maximum expected hail size are presented in this paper.

The prediction of maximum expected hail size depends on the vertical integration of an empirical function of maximum reflectivity values ≥40 dB*Z*. Plots of maximum expected hail size are found in Fig. 3. For at least 97% of the cells, data points fall on the diagonal 1:1 line (left panels) or horizontal zero difference line (right panels). As listed in the bottom-right corner of the left panels, about half of those data are at the (0, 0) point where maximum expected hail size is zero. Nearly equally scattered on both sides of the line are the few points that do not have the same values for the two VCPs. The typical extreme size differences are only 0.6 cm (0.25 in.).

Probability of hail (POH) of any size is computed as a function of the height of the 45-dB*Z* echo above the environmental 0°C level. On the other hand, the probability of severe hail (POSH; diameter ≥1.9 cm or 0.75 in.) depends on the vertical integration of an empirical function of maximum reflectivity values ≥40 dB*Z* and the 0°C level (Witt et al. 1998). The distributions of POH and POSH (not shown) are very similar to those

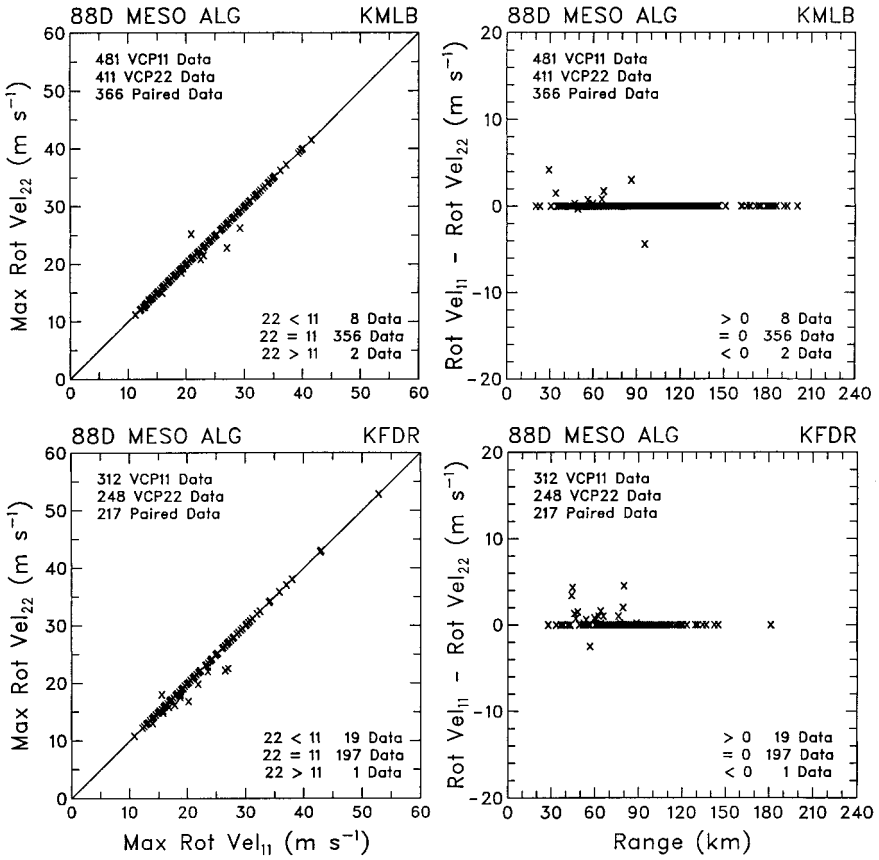


FIG. 5. Plots of maximum rotational velocity and velocity differences between VCP 11 and VCP 22 for data collected by KMLB and KFDR. The plots are based on the WSR-88D mesocyclone algorithm.

for maximum expected hail size. Typical differences in probability between the two VCPs are about ±10%.

### *c. WSR-88D mesocyclone algorithm*

The WSR-88D mesocyclone algorithm identifies cyclonic circulations that exceed specified shear and height criteria. Four parameters produced by the algorithm were investigated: mesocyclone depth, maximum rotational velocity, maximum azimuthal shear across the mesocyclone, and the integrated rotational strength index. Only plots of mesocyclone depth and maximum rotational velocity using VCP 11 and VCP 22 are presented in this paper.

Mesocyclone depth is computed over a depth where the shear exceeds a specified threshold value; the algorithm allows a gap of one elevation angle where the shear drops below the threshold value. Shown in Fig. 4 are plots of mesocyclone depth. Of the depths that are not the same for the two VCPs, those computed from VCP 11 are usually greater. One would expect to find this type of relationship because the top of the mesocyclone feature, at times, will occur at the height of a missing elevation angle in VCP 22.

The algorithm computes the rotational velocity at a given elevation angle as one-half the difference between the maximum Doppler velocity value and the minimum Doppler velocity value across the mesocyclone signature. The maximum rotational velocity for the three-dimensional feature is the maximum of the rotational velocities at the various elevation angles. Shown in Fig. 5 are plots of the maximum rotational velocity. Differences in maximum rotational velocity between the two VCPs are minimal. Where differences occur, the VCP 11 values are usually greater than the VCP 22 values.

The algorithm computes shear, at a given elevation angle, as the difference between the extreme Doppler velocity values across the mesocyclone signature divided by the distance between the extreme values. Plots of the maximum shear values throughout the mesocyclone depth (not shown) reveal that only a few percent of the shear values are not the same for the two VCPs. Where there are differences, VCP 11 values are larger in almost all cases.

A rotational strength index is computed from a nomogram based on the rotational velocity and diameter of the mesocyclone signature at a given elevation angle (Lee and White 1998). The integrated rotational strength

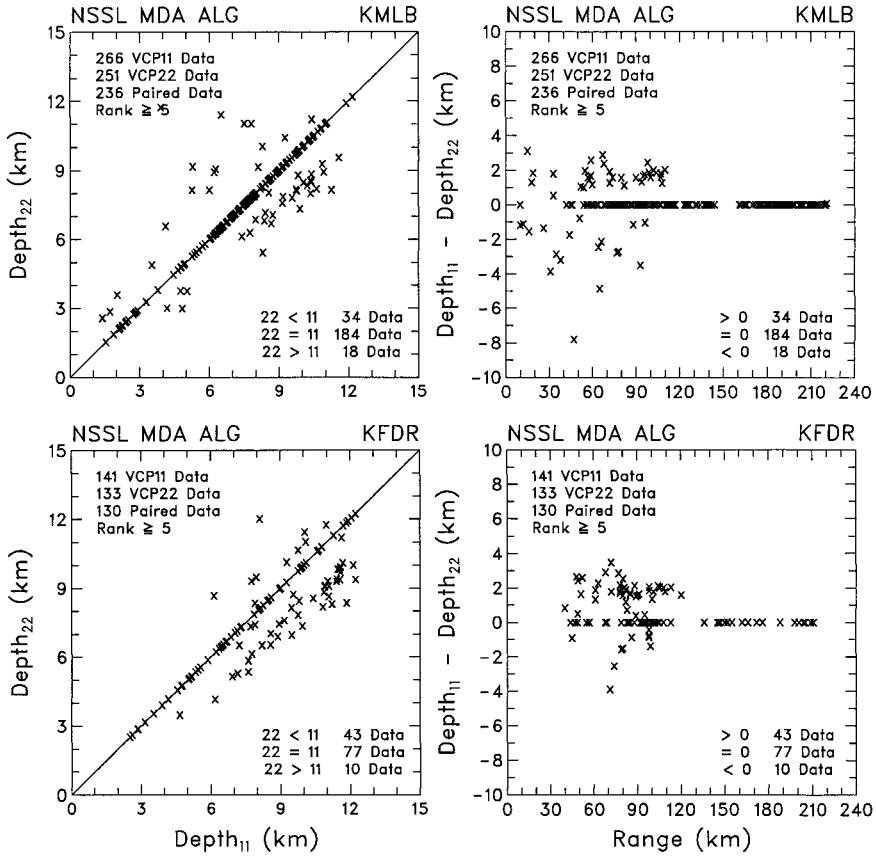


FIG. 6. Plots of mesocyclone depth and depth differences between VCP 11 and VCP 22 for data collected by KMLB and KFDR. The plots are based on the NSSL mesocyclone detection algorithm.

(IRS) index is the sum of the individual rotational strength index values with height. Plots (not shown) reveal that where there are differences, larger IRS index values usually are associated with VCP 11. Again, this situation is to be expected owing to the missing elevation angles with VCP 22.

### *d. NSSL mesocyclone detection algorithm*

The NSSL MDA is a not-yet-operational enhancement of the WSR-88D mesocyclone algorithm (Stumpf et al. 1998). Five parameters produced by the NSSL algorithm were investigated: mesocyclone depth, maximum rotational velocity, maximum azimuthal shear across the mesocyclone, three-dimensional mesocyclone strength rank, and mesocyclone strength index (MSI). Only plots of mesocyclone depth, maximum rotational velocity, and MSI are presented.

The NSSL MDA assigns a two-dimensional (2D) strength rank to the mesocyclone signature at each elevation angle. Rank is based on threshold values of both the Doppler velocity difference across the signature and the shear across the signature; for details see Stumpf et al. (1998). Threshold values decrease with increasing range to reflect sampling problems associated with the broadening of the radar beam with range. The overall strength rank for the three-dimensional (3D) mesocyclone is determined by finding the strongest continuous vertical core of 2D features whose 2D strength ranks are greater than or equal to a given strength rank. This core must exceed a depth criterion, and the base of the core must be below 5 km (16.4 kft). Only mesocyclones having a 3D strength rank of at least 5 were compared.

The algorithm computes mesocyclone depth from the unbroken sequence of elevation angles on which a two-dimensional mesocyclone signature is identified. Since the NSSL algorithm can detect weaker mesocyclone signatures than can the WSR-88D algorithm, vertical gaps do not need to be considered in establishing the vertical continuity of a feature. Plotted in Fig. 6 are mesocyclone vertical depths from the NSSL algorithm. These depths are considerably greater than those for the WSR-88D mesocyclone algorithm (Fig. 4) because the WSR-88D algorithm does not permit mesocyclone signatures to exist at heights greater than 8 km (default value) above the radar.

The NSSL MDA is more realistic than its WSR-88D counterpart in finding the peak Doppler velocity values

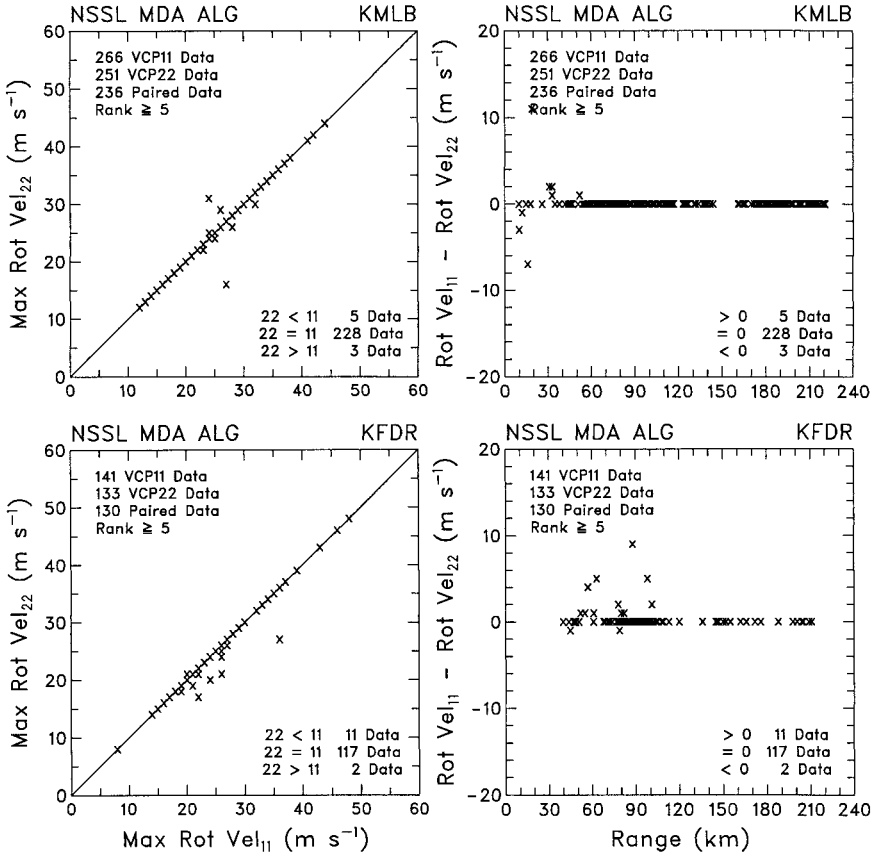


FIG. 7. Plots of maximum rotational velocity and velocity differences between VCP 11 and VCP 22 for data collected by KMLB and KFDR. The plots are based on the NSSL mesocyclone detection algorithm.

of the mesocyclone signature. The NSSL algorithm allows for small-scale fluctuations in the velocity field as the algorithm proceeds from the velocity minimum in search of the velocity maximum; see Stumpf et al. (1998). This approach produces more representative values of maximum rotational velocity, mesocyclone core diameter, and maximum shear.

Plotted in Fig. 7 are the maximum rotational velocities from the NSSL algorithm. Differences in values between the two VCPs are not very great and are comparable to those found with the WSR-88D algorithm (Fig. 5). For most of the differences, VCP 11 values are greater than those for VCP 22, as one would expect.

An MSI is computed by vertically integrating the strength rank of each 2D feature, which is weighted by the air density at the height of the feature. This means that more weight is given to 2D features at lower heights. To normalize the MSI values for a variety of mesocyclone depths, the MSI is divided by the total 3D depth of the feature. For MSI values (Fig. 8), about 30%–40% of the paired values are different for the two VCPs. Usually, the VCP 11 values are greater.

For maximum shear values from the NSSL MDA (not presented), about 10% of the paired values are different for the two VCPs, which is much greater than for the WSR-88D algorithm. In nearly all cases, the VCP 11 shears are greater than those for VCP 22.

For the 3D strength ranks (not presented), only about 3% of the values are not the same for the two VCPs, and for most of these, the VCP 11 value is greater. If some larger 2D strength ranks were at the missing elevation angles of VCP 22, one would expect the 3D values for VCP 22 to be less than or equal to those for VCP 11.

### *e. NSSL tornado detection algorithm*

NSSL designed the new TDA to identify locally intense vortex signatures associated with tornadoes (Mitchell et al. 1998). Brown et al. (1978) pointed out that when the radar beam is larger than the tornado, a degraded signature of the tornado is evident in the Doppler velocity measurements. They called the degraded signature a tornadic vortex signature (TVS). This algorithm divides the TVS into two subcategories: TVS and elevated TVS (ETVS). The algorithm defines a TVS as a 3D detection that meets minimum strength

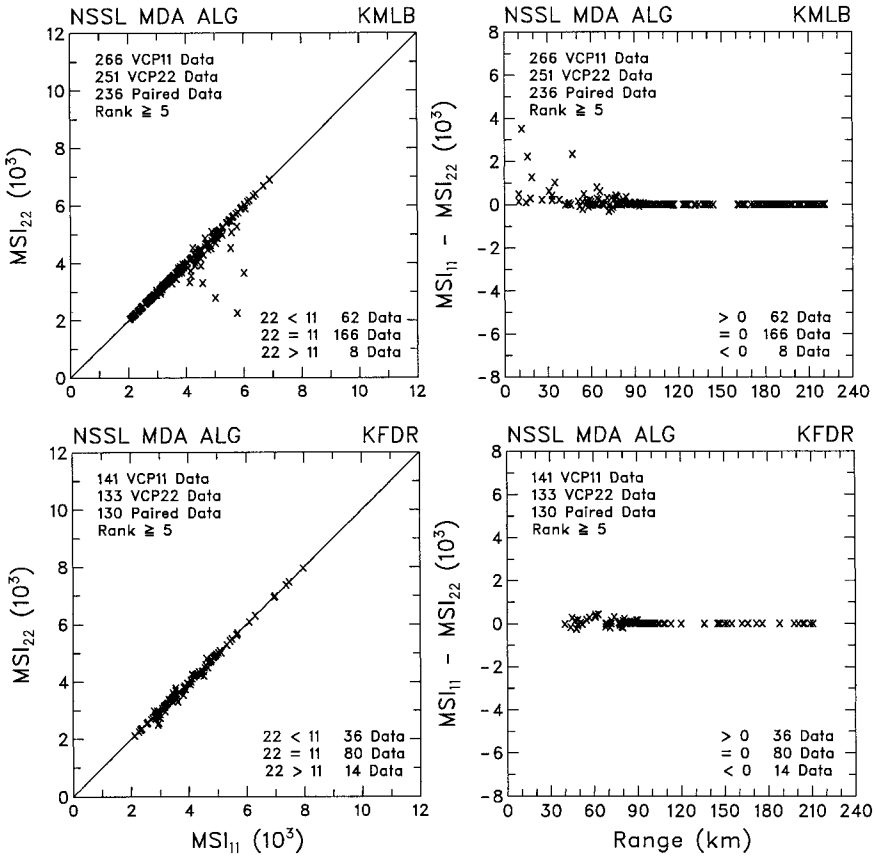


FIG. 8. Plots of MSI and differences in index values between VCP 11 and VCP 22 for data collected by KMLB and KFDR. The plots are based on the NSSL mesocyclone detection algorithm.

and depth criteria and whose base extends downward to the 0.5° elevation angle or to a prescribed height above the radar antenna (currently 600 m). An ETVS is a 3D detection that meets all the TVS criteria except the base elevation or altitude criterion (Mitchell et al. 1998).

Three algorithm parameters were investigated: TVS depth, maximum gate-to-gate azimuthal velocity difference, and maximum azimuthal shear. The results include both TVS and ETVS occurrences. Only plots of TVS depth and maximum gate-to-gate azimuthal velocity difference using VCP 11 and VCP 22 are presented here.

The vertical depth of a 3D TVS/ETVS is defined by at least two adjacent elevation angles that have vertically correlated 2D features; no more than one gap, where data are missing or the prescribed 2D vortex criteria are not met, is allowed in the vertical. For TVS/ETVS depths (Fig. 9) based on VCP 11 and VCP 22, about 20%–35% of the data points are different for the two VCPs. In a vast majority of these cases, VCP 11 depths are greater than VCP 22 depths. These differences would occur if part of the 3D TVS/ETVS occurs at an elevation angle that is missing in VCP 22. In both Florida and Oklahoma, the algorithm identified TVS/ETVSs at ranges up to about 150 km (80 n mi).

The conventional feature that indicates the presence of a TVS/ETVS in the Doppler velocity display at a given elevation is a marked 2D Doppler velocity difference at range gate locations that are adjacent in azimuth. Plotted in Fig. 10 are the maximum gate-to-gate azimuthal Doppler velocity differences in 3D features for VCP 11 and VCP 22. With few exceptions, the velocity differences are the same for both VCPs. Where there are VCP differences, VCP 11 values are larger in nearly every instance.

The azimuthal shear associated with a TVS/ETVS is defined as the Doppler velocity difference at azimuthally adjacent range gates (i.e., gate-to-gate difference) divided by the azimuthal distance between the two gates. For maximum azimuthal shear values within the 3D TVS/ETVS (not shown), the vast majority of values are the same for the two VCPs. When there are differences, VCP 11 values are nearly always larger.

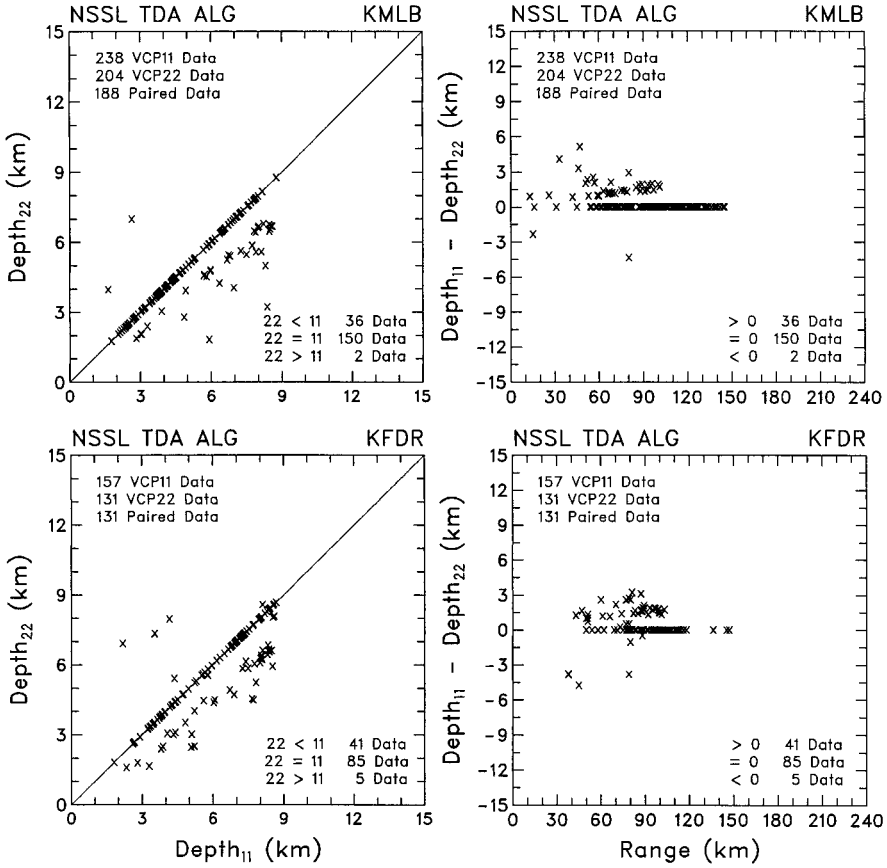


FIG. 9. Plots of TVS/ETVS depth and differences in depth values between VCP 11 and VCP 22 for data collected by KMLB and KFDR. The plots are based on the NSSL tornado detection algorithm.

*f. Velocity azimuth display algorithm*

When a Doppler radar makes a 360° scan at a constant elevation angle, and there is sufficient radar return at a given slant range over portions of the scan, it is possible to retrieve the mean wind direction and speed around the slant range circle centered on the radar location (Lhermitte and Atlas 1961). Using the VAD algorithm, one can obtain a vertical profile of wind direction and speed from the full set of elevation angles specified by a given VCP. The WSR-88D VAD algorithm constructs the vertical profile at a default range of 30 km (16.2 n mi). Once the heights for the profile are specified, the algorithm uses the elevation angle that is closest to the 30-km range at each height for the wind computations.

Plotted in Fig. 11 are the VAD wind directions for VCP 11 and 22. The plots on the left show some scatter about the 1:1 line. The plots on the right reveal the reason for the scatter. VAD wind directions computed from the elevation angles that are common to both VCPs are the same. However, at heights corresponding to the missing VCP 22 elevation angles, the wind directions are different. The differences arise when, at a given height, the VCP 22 elevation angle closest to the range of 30 km is different from the closest VCP 11 elevation angle. Most VCP 22 wind directions are within ±10° of the VCP 11 directions.

As with wind direction, the VAD-derived wind speed differences (not shown) occur at the heights of the missing elevation angles in VCP 22. Most VCP 22 wind speeds are within ±3–4 m $s^{-1}$ (6–8 kt) of the VCP 11 speeds.

## 4. Concluding comments

When using WSR-88D data to monitor severe weather events in preparation for issuing warnings, forecasters use one of two volume coverage patterns. VCP 11 consists of 14 elevation scans (ranging from 0.5° to 19.5°) in 5 min. VCP 21 consists of nine elevation scans (also ranging from 0.5° to 19.5°) in 6 min. The coarser vertical and temporal resolution of VCP 21 raises questions about its ability to adequately sample severe storms. The purpose of this paper is to inves-

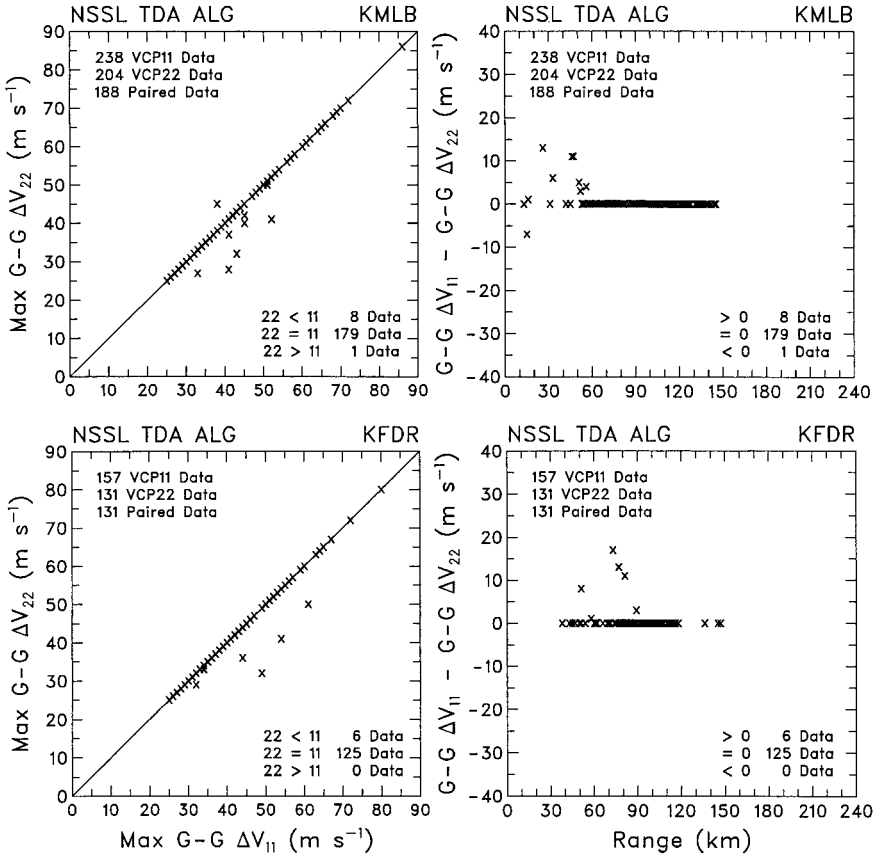


FIG. 10. Plots of maximum gate-to-gate azimuthal Doppler velocity differences and differences in the velocity difference values between VCP 11 and VCP 22 for data collected by KMLB and KFDR. The plots are based on the NSSL tornado detection algorithm.

tigate the effects of the vertical resolution of the two VCPs on the output from various WSR-88D and NSSL prototype algorithms.

VCP 11 was modified by deleting five elevation angles, so the remaining elevation angles closely resemble VCP 21 (see Table 1). The modified VCP was called VCP 22. Using VCP 22 as a proxy for VCP 21, algorithm output was compared using VCP 11 and VCP 21/22. Considering that some elevation angles present in VCP 11 are missing from VCP 21/22, the algorithm output is found to be noticeably compromised.

The data presented in Figs. 1–10 show that algorithm outputs from VCP 11 and VCP 22 are identical at far ranges where elevation angles are below 5°, that is, where VCP 11 and VCP 21/22 have common elevation angles (Table 1). However, differences in values of algorithm parameters can occur when the heights of specific parameters are above 5° elevation. From the data presented in the figures, it is not obvious how many paired data points are above 5° elevation.

Figure 12 was prepared to investigate the percentage of paired data points above 5° that are different. The figure does not include the following six algorithm parameters because the height of the maximum value, from which an elevation angle could be computed, was not available: probability of hail (not shown), maximum rotational velocity (Fig. 5), and maximum shear (not shown) from the WSR-88D mesocyclone algorithm and strength rank (not shown) from the NSSL mesocyclone detection algorithm. The five parameters with asterisks in Fig. 12 are those derived through vertical integration of various quantities and, therefore, do not have a height associated with them. To compute representative elevation angles for the parameters with asterisks, the 30-dB*Z* height was used as the top of the VIL and hail parameters; the respective heights of mesocyclone tops were used for the WSR-88D and NSSL mesocyclone parameters. The number of paired data points that were different for each parameter are listed in the third column in the figure.

The bars in Fig. 12 show that, on the average, over half of the paired data points above 5° elevation derived from VCP 21/22 are different from those derived from VCP 11. The hail parameters are the only ones that are

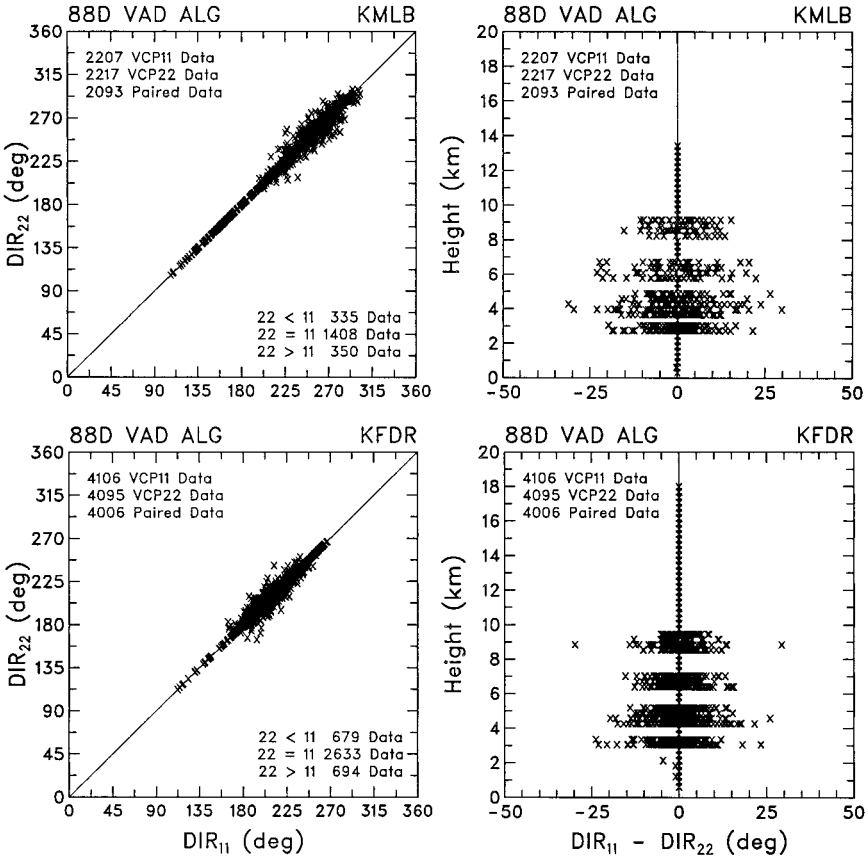


FIG. 11. Plots of VAD wind direction and direction differences between VCP 11 and VCP 22 for data collected by KMLB and KFDR. Heights are relative to sea level.

not seriously affected by VCP 21/22, with only 10%–20% of the values being different. For the various depth and height parameters, 50%–80% of the paired data points are different. VAD wind speeds and directions are different in about half of the cases.

The degradation in vertical resolution associated with VCP 21/22 affects algorithm parameters that forecasters depend upon for issuing severe thunderstorm and tornado warnings. For example, VIL is a parameter used to monitor storm severity. The bars in Fig. 12 show that VIL computations based on VCP 21/22 differ from those based on VCP 11 70%–80% of the time at ranges where 30-dB*Z* tops are above 5°. Since VCP 21/22 can overestimate VIL by 10–20 kg $m^{-2}$ or more, there is a chance that forecasters will overwarn on storms when using VCP 21.

Mesocyclone and tornadic vortex signatures also play an important role in the issuance of warnings. The bars in Fig. 12 show that parameters from the various mesocyclone and tornado detection algorithms based on VCP 21/22 at elevation angles greater than 5° differ from those based on VCP 11 50%–100% of the time. These discrepancies arise owing to the vertical data gaps in VCP 21 relative to VCP 11. When there are gaps, extreme values can be missed, leading to underestimates of the strength of mesocyclone and tornadic vortex signatures. Also, gaps appearing at the top of features can lead to the underestimation of mesocyclone or TVS depth. This, in turn, could mean that the algorithm does not identify the vortex as a mesocyclone or TVS because it does not satisfy the depth criteria.

The deficiencies associated with VCP 21 could mislead forecasters into not issuing warnings that should have been issued or issuing warnings that should not have been issued. This study indicates that one should use VCP 11 as the scanning strategy when severe storm features of interest are at elevation angles greater than 5°. The faster turnaround time of VCP 11 has the additional advantage of being able to better monitor fast-evolving events. Based on these indications, an objective study should be conducted to determine how the use of VCP 11 and VCP 21 affect decisions made by forecasters as part of the warning decision process.

*Acknowledgments.* This study was supported through a memorandum of understanding between the National

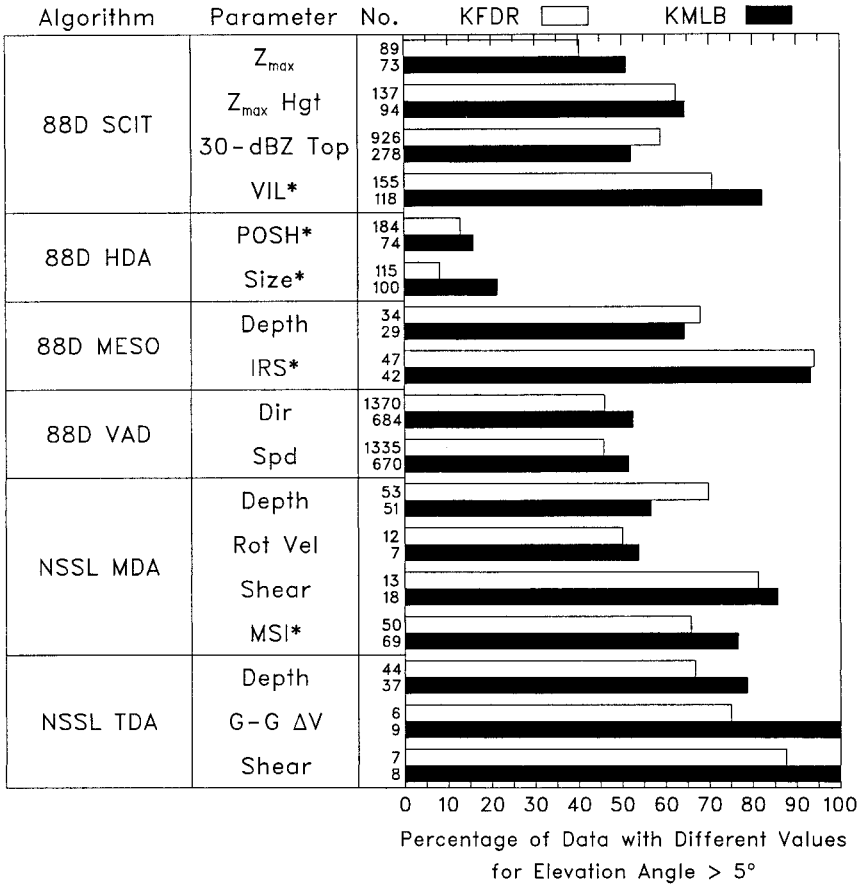


FIG. 12. Percentage of algorithm parameter values that were different using VCP 11 and VCP 21/22 when the elevation angle of the parameter was greater than 5°; missing elevation angles above 5° associated with VCP 21/22 produce the different values. The numbers in the third column are the numbers of paired data points that were different for each radar. Asterisks indicate those parameters that arise from vertical integration; see the text for additional comments.

Severe Storms Laboratory and the National Weather Service WSR-88D Operational Support Facility (OSF). We appreciate discussions with Robert Lee, Randy Steadham, Dale Sirmans, and other OSF staff members. Comments made by Arthur Witt and Terry Schuur of NSSL and by the anonymous reviewers improved the clarity of this manuscript.

## REFERENCES

Brown, R. A., L. R. Lemon, and D. W. Burgess, 1978: Tornado detection by pulsed Doppler radar. *Mon. Wea. Rev.*, **106,** 29–38.

Greene, D. R., and R. A. Clark, 1972: Vertically integrated liquid: A new analysis tool. *Mon. Wea. Rev.*, **100,** 548–552.

Johnson, J. T., P. L. MacKeen, A. Witt, E. D. Mitchell, G. J. Stumpf, M. D. Eilts, and K. W. Thomas, 1998: The storm cell identification and tracking algorithm: An enhanced WSR-88D algorithm. *Wea. Forecasting,* **13,** 263–276.

Lee, R. R., and A. White, 1998: Improvement of the WSR-88D mesocyclone algorithm. *Wea. Forecasting,* **13,** 341–351.

Lhermitte, R. M., and D. Atlas, 1961: Precipitation motion by pulse Doppler radar. *Proc. Ninth Weather Radar Conf.,* Kansas City, MO, Amer. Meteor. Soc., 218–223.

Mahoney, E. A., and R. Schaar, 1993: WSR-88D scan strategy impacts on the vertically integrated liquid product. Preprints, *26th Int. Conf. on Radar Meteorology,* Norman, OK, Amer. Meteor. Soc., 44–46.

Mitchell, E. D., S. V. Vasiloff, G. J. Stumpf, A. Witt, M. D. Eilts, J. T. Johnson, and K. W. Thomas, 1998: The National Severe Storms Laboratory tornado detection algorithm. *Wea. Forecasting,* **13,** 352–366.

Stumpf, G. J., A. Witt, E. D. Mitchell, P. L. Spencer, J. T. Johnson, M. D. Eilts, K. W. Thomas, and D. W. Burgess, 1998: The National Severe Storms Laboratory mesocyclone detection algorithm for the WSR-88D. *Wea. Forecasting,* **13,** 304–326.

Witt, A., 1997: Variations in algorithm output for the same storm viewed by different WSR-88Ds. Preprints, *28th Conf. on Radar Meteorology,* Austin, TX, Amer. Meteor. Soc., 497–498.

——, M. D. Eilts, G. J. Stumpf, J. T. Johnson, E. D. Mitchell, and K. W. Thomas, 1998: An enhanced hail detection algorithm for the WSR-88D. *Wea. Forecasting,* **13,** 286–303.